

Comparison of Meteor Radar and Na Doppler Lidar Measurements of Winds in the Mesopause Region Above Maui, HI

S. J. Franke, X. Chu, A. Z. Liu

Department of Electrical and Computer Engineering, University of Illinois at
Urbana-Champaign

W. K. Hocking

University of Western Ontario, London, Ontario

S. J. Franke, X. Chu, A. Z. Liu Department of Electrical and Computer Engineering, University of Illinois, Urbana, Illinois 61802, USA. (e-mail: s-franke@uiuc.edu)

W. K. Hocking, Department of Physics, The University of Western Ontario, London, Ontario N6A 5B7, Canada

Abstract. Simultaneous sodium (Na) Doppler lidar and meteor radar measurements of horizontal winds in the mesopause region over Maui, HI were collected in July, 2002 and October/November 2003. The coincident measurements span 96 hours and altitudes between 80-100 km. Statistical comparisons are carried out on radar/lidar winds with 1 h and 4 km time and height resolution, respectively. The rms radar/lidar wind component differences observed in this study are in the range 12-17 m/s at altitudes below 96 km. This is smaller than the rms differences observed in a previous Na lidar and meteor radar comparison. Lidar wind component variances exceed radar variances, and radar/lidar covariance is nearly equal to the radar variance. Excess variance observed by the lidar is consistent with the fact that the meteor radar cannot resolve wind perturbations with horizontal scales smaller than ~ 200 km, whereas the lidar will respond to all horizontal scales. Close correspondence between the radar wind variance and radar/lidar covariance suggests that measurement errors associated with the radar winds are swamped by geophysical variation. Furthermore, the excess lidar variance exceeds lidar estimation errors by a large factor, indicating that the lidar measurement errors are also insignificant relative to geophysical variations. Together, these observations suggest that the observed radar/lidar differences are a consequence of the different horizontal wavenumber filters associated with the techniques and, hence, the differences are determined by the strength and shape of the horizontal wavenumber spectrum for wind perturbations at scales smaller than ~ 200 km.

1. Introduction

Joint measurement campaigns involving all-sky airglow imagers, high resolution Na Doppler lidar, and a meteor radar were carried out in July, 2002 and October/November 2003 under the auspices of the Maui Mesosphere and Lower Thermosphere (Maui MALT) initiative. The meteor radar was deployed at Maui to provide temporally continuous measurements of mesopause-region winds, which provide an essential context for interpreting lidar and airglow imager measurements of gravity waves propagating through the region.

During these campaigns, the University of Illinois (UIUC) meteor radar and UIUC Na Doppler lidar operated simultaneously for approximately 96 nighttime hours, providing an opportunity to study the consistency between mesopause-region winds measured by these instruments. This paper describes the characteristics of, and data analysis techniques employed by, the new UIUC Maui Meteor Radar, and a detailed statistical comparison of horizontal wind components measured by the Na Doppler lidar and meteor radar in the 80-100 km altitude range. The radar/lidar comparison reported here follows an earlier comparison between UIUC Na Doppler lidar winds and meteor radar winds (*Liu et al.*, 2002) collected at Starfire Optical Range (SOR) in New Mexico.

This paper is organized as follows. Descriptions of the meteor radar and Na Doppler lidar are provided in section 2. Descriptive statistics summarizing the differences between the lidar and radar measurements of zonal and meridional wind components are presented in section 3. The results are interpreted in section 4. Finally, in section 5 the results are summarized and compared with earlier lidar/meteor radar comparison.

2. Instrument Descriptions

2.1. Meteor Radar

The UIUC Maui/MALT meteor radar is located in Kihei on Maui, HI at 20.75°N, 156.43°W. The system is a SKiYMET radar (*Hocking et al.*, 2001) operating at 40.92 MHz. A single 3-element Yagi antenna directed towards the zenith is used to illuminate meteor trails. Meteor trail reflections are coherently detected on five 3-element Yagi antennas oriented along two orthogonal baselines, with one antenna in the center of the array common to both baselines. On each baseline, the outer antennas are separated from the center antenna by 1.5 and 2.0 wavelengths, respectively. This configuration minimizes antenna coupling, provides enough redundancy to unambiguously determine the azimuth and elevation of most echoes, and provides excellent angular resolution for position determination. The average transmitted power is approximately 170 W, resulting from a 13.3 μ s pulse length, 6 kW peak envelope power, and an interpulse period (IPP) of 466 μ s. Returns are sampled every 13.3 μ s, resulting in 2 km range resolution. The relatively short IPP causes meteor echoes to be aliased in range, however the narrow height distribution of meteor echoes, combined with precise azimuth/elevation angle measurement, allows most range ambiguities to be resolved. Algorithms employed for determining meteor trail position and Doppler shift are described in detail in *Hocking et al.* (2001).

Wind velocities are estimated from the trail positions and Doppler shifts using a weighted least-squares fit, assuming a constant wind vector composed of eastward and northward components. The vertical wind component is neglected. Thus, the fitting procedure determines horizontal components (u, v) by minimizing the weighted residual

$$\chi^2 = \sum_i \left(\frac{v_r^i - ul^i - vm^i}{\sigma^i} \right)^2, \quad (1)$$

where v_r^i is the measured line-of-sight velocity, and $l^i = \sin \theta^i \cos \phi^i$, $m^i = \sin \theta^i \sin \phi^i$ are components of a unit vector directed along the line-of-sight to the detected meteor trail. The zenith angle and azimuth angle of the i 'th meteor trail are denoted by θ^i and ϕ^i , respectively.

The wind-vector fit is based on echoes collected within 1 hour time bins. The height resolution that can be achieved by the meteor radar is limited by uncertainty in the measured distance to the meteor trail and in the estimated zenith angle of the detected meteor trails. In terms of the rms uncertainties in distance (σ_r) and zenith angle (σ_θ) the rms height uncertainty for a trail located at height h and zenith angle θ is approximately

$$\sigma_h = \sqrt{\sigma_r^2 \cos(\theta)^2 + h^2 \sigma_\theta^2 \tan(\theta)^2}. \quad (2)$$

Assuming range errors uniformly distributed over ± 2 km, then $\sigma_h = 1.33$ km. The rms zenith angle error is expected to be $\sim 1^\circ - 2^\circ$ *Jones et al.* (1988). Most returns are detected from zenith angles in the range $40 - 60^\circ$. For meteors at the most probable height (90 km) and zenith angle (50°), the height uncertainty is therefore $\sim 2.2-3.9$ km. The uncertainty is smaller for smaller zenith angles, and is smallest for returns directed at the zenith. In view of these considerations, the meteor data was binned into height bins of width 4 km. For the statistical comparisons discussed herein, we estimated the wind components at 5 heights using bins centered at altitudes of 82 km, 86 km, 90 km, 94 km, and 98 km. The bins corresponding to these altitudes do not overlap; this will ensure that statistical estimation errors at adjacent heights are independent, and simplify the interpretation of the results. Horizontal wind vectors were estimated when at least 6 meteor echoes were available in a 1 hour x 4 km time/height bin.

Within a particular altitude bin, the contribution from each trail is weighted by a term that depends on zenith angle, θ^i , and distance, r^i . The inverse of the weighting coefficient, denoted by σ^i in equation (1), is defined by

$$(\sigma^i)^2 = (\sigma_S^2 \sigma_r^2 + \sigma_w^2) \cos^2 \theta^i + (r_i^2 \sigma_S^2 \sigma_\theta^2 + \sigma_u^2) \sin^2 \theta^i. \quad (3)$$

In (3) the parameters r^i and θ^i represent the measured range and zenith angle of the i 'th meteor echo. The σ 's on the right-hand side represent rms uncertainties in measured range and zenith angle (in radians) of the meteor echo (σ_r , σ_θ), and rms spatial/temporal variations of the actual wind field with respect to the purely horizontal and uniform wind vector assumed for the fitting procedure (σ_u , σ_w , σ_S).

The error model, equation (3), is supposed to explain the variance of the observed meteor trail line-of-sight velocity around its expected value. The first term dominates for echoes detected at small zenith angles, where the measured line-of-sight trail velocity deviates from the value predicted by the constant horizontal wind model due to contributions from the vertical wind component (with rms variability σ_w) and from error in determining the height of the echo in the presence of vertical wind shear. If the rms wind shear for either component of the horizontal wind is denoted by σ_S , where $\sigma_S^2 = \langle (\frac{\partial u}{\partial z})^2 \rangle = \langle (\frac{\partial v}{\partial z})^2 \rangle$, and the uncertainty in measured distance to the meteor trail is σ_r , then the rms residual due to height-errors in the presence of wind-shear is $\sigma_S \sigma_r \cos \theta$.

The second term in equation (3) is dominant for echoes detected at large zenith angles, where residuals arise from deviations of the horizontal wind from the constant modeled value and from a height-error/wind-shear contribution arising from errors in the estimated zenith angle of the echo. We assume that the zonal and meridional wind have equal rms deviations, σ_u , so that the rms error due to the fluctuating component of the horizontal

wind is $\sigma_u \sin \theta$. If the zenith angle associated with the meteor echo is estimated with rms error σ_θ , then the resulting height error is approximately $r\sigma_\theta \sin \theta$, so the product of height-error and rms wind-shear is $r\sigma_\theta\sigma_S \sin \theta$.

Several other error terms, all of which are expected to be relatively small compared to the terms discussed above, have been ignored. In particular, it should be noted that the rms uncertainty of the estimated meteor trail radial velocity was not included in equation (3). This term is calculated in practice from the radial velocities obtained using each of the 5 receiver channels. When the rms uncertainty of the radial velocity exceeds 7 m/s, the meteor echo is discarded. The median rms uncertainty of the remaining radial velocity measurements, which are used for wind estimation, is a few m/s. Hence, this term is negligible compared to the terms already included in equation (3). The numerical values of the weighting function parameters employed for our fits are summarized in Table 1. The rms zenith angle and range errors were determined as described earlier. The rms vertical and horizontal winds and rms wind shear were adjusted to simultaneously minimize the rms differences between radar and lidar winds and to normalize the mean-square residual to unity, i.e. we force $\langle \chi^2 \rangle \simeq 1$. It is important to note that the numerical values used for these parameters were adjusted to force the error model into compliance with the observed rms residuals by requiring that the ensemble mean value of χ^2 , taken over the entire data set, is approximately unity, i.e. $\langle \chi^2 \rangle \simeq 1$. As such, the numerical values σ_w , σ_u , σ_S given in Table 1 should not be taken as formal estimates of these parameters.

Table 1

We have carried out numerous comparisons between the lidar wind and the radar wind and have verified that the weighting function described here results in smaller rms radar/lidar differences than does either an unweighted fit with fixed zenith angle limits, or

fits based on equation (3) but with radically different numerical values for the parameters given in Table 1.

2.2. Na Doppler lidar

The UIUC Na wind/temperature lidar is installed at the Air Force Research Laboratory AEOS facility on Maui, at the peak of Haleakala, at coordinates 20.71°N, 156.26°W. The laser is coupled to a 3.7 m steerable astronomical telescope through the coude path so that the beam can be pointed at any direction. A 0.6 m diameter portion of the telescope primary mirror is used to project the laser beam, while the remainder is used for collecting backscattered light and focusing it onto the detector. The beam divergence is approximately 0.4 mrad, which produces a beam diameter (full width @ e^{-2}) of 40 m at a range of 100 km. The laser transmitter is pulsed at 50 pps, and the measured laser output power varies between 1 and 2 W. The laser beam is coupled to the telescope primary mirror through the coude optical system, which is also shared with the lidar detector. We estimate that the coupling efficiency is at least 50%, so that the actual laser power transmitted into the atmosphere varies between about 0.5 and 1 W. In this configuration, temperature and radial wind can be measured along the laser beam. The lidar is pointed at zenith (Z) and 30° off-zenith to the north (N), south (S), east (E) and west (W) in the following sequence ZNEZSW. At each position, backscattered photocount profiles are obtained at three frequencies (peak, plus and minus), with a 90 second integration time and 24 m range resolution. The laser frequencies are controlled by an acousto-optic modulator, and the frequency is shifted every 50 pulses, or once per second. Approximately 30 s are required to steer the telescope to the next position. This 6-position sequence is completed about every 12 minutes so the complete wind and temperature field can be derived every

6 min. To increase signal to noise ratio, the raw wind and temperature data are derived at a height resolution of 480 m. The horizontal wind at each direction (NSEW) was derived by dividing the radial wind by $\sin(30^\circ)$. The vertical wind component in the radial wind is assumed to be negligible.

3. Results from 2002 and 2003 Campaigns

Simultaneous radar/lidar wind measurements are available for 5 nights in July, 2002 and 7 nights in October/November 2003. Approximately 96 hours of simultaneous wind measurements are available. For statistical comparisons with the radar winds, the time and height resolution of the lidar winds were degraded with filters to match those of the meteor radar winds. This was accomplished by averaging the lidar winds in 1 hour blocks, and by averaging the data in height over bins of width 4 km, centered at the same altitudes used for estimating the radar winds. While it is possible to match the temporal and height resolutions of the two instruments using these filters, the two instruments sample the wind field differently in the horizontal plane, and hence the instruments have significantly different effective horizontal wavenumber response functions. The lidar samples the line-of-sight wind component at five points, and each sample represents a spatial average over the spot illuminated by the lidar, which has a diameter of approximately 40 meters. The meteor radar estimates winds using meteor trail echoes distributed randomly over a horizontal region with diameter ~ 200 km. As such, wind perturbations with scales comparable to, or smaller than, this dimension will not be resolved by the radar. Therefore, the portion of the horizontal wavenumber spectrum for horizontal wind perturbations corresponding to scales smaller than ~ 200 km will contribute to observed variance in the lidar winds, but not to the radar winds. In the absence of instrumental measurement

errors, the lidar winds should exhibit more variance than the radar winds, and the excess lidar variance will correspond to the variance expected for radar/lidar wind differences. Instrumental measurement errors will add additional contributions to the variance of the radar/lidar wind difference. We shall examine the relative importance of contributions from measurement errors and difference in horizontal wavenumber response functions later in the paper.

To illustrate the nature of the data set, sample height profiles of meridional and zonal wind components measured simultaneously by the two instruments are plotted in Figure 1, where the lidar profiles are marked with circles and the radar measurements are plotted with asterisks. As noted earlier, the profiles have 1 hour and 4 km time and height resolution, respectively. The profiles have been over-sampled at a 1 km height interval for these plots. In general, strong correspondence between the meteor and lidar wind profiles is evident.

Figure 1

Scatter plots of all coincident radar/lidar winds from all 5 altitude bins are plotted in Figure 2, and histograms of lidar/radar wind component differences are shown in Figure 3. The statistical moments of the joint data set are summarized in Table 2.

Figure 2**Figure 3****Table 2**

Referring to Table 2, the mean radar/lidar wind component differences are 0.4 m/s (meridional) and 0.6 m/s (zonal). Since the difference histograms shown in Figure 3 indicate some noticeable deviation from the normal distribution (plotted with the smooth line), we determined 99% confidence intervals for the mean differences using the bootstrap procedure described in *Efron and Tibshirani* (1998). In particular, we used 500 bootstrap replications and determined the 0.5 and 99.5 percentiles of the bootstrap distribution of radar/lidar wind component mean differences. The confidence intervals are [-1.6 m/s,

2.4 m/s] (meridional) and [-1.5 m/s, 2.9 m/s] (zonal). In both cases the 99% confidence interval for the radar/lidar mean differences includes zero, indicating that there is no significant difference between the radar and lidar mean winds.

The median radar/lidar differences were found to be 0.8 m/s (meridional) and -0.2 m/s (zonal). The Wilcoxin signed-rank sum test was used to test the hypothesis that the observed median differences arise from a population with nonzero median (*Wilcoxin*, 1945). The Wilcoxin test indicates that the observed medians are not significantly different from zero at the 5% level (the probabilities calculated using the Wilcoxin test were 22% (meridional) and 78% (zonal)). Thus, we conclude that the mean and median differences are not significantly different from zero.

The variance of the lidar wind components are 12% (meridional) and 7% (zonal) larger than the corresponding radar values. Radar/lidar covariances are nearly equal to the radar variances, resulting in a correlation of 0.91 between the radar/lidar meridional components and 0.89 between the zonal components. The median absolute value of the radar/lidar wind component difference is 8.4 m/s (meridional) and 9.0 m/s (zonal), i.e. half of all coincident radar/lidar meridional (zonal) wind component pairs differ by more/less than 8.4 m/s (9.0 m/s). The rms radar/lidar differences are approximately 16 m/s (meridional) and 17 m/s (zonal).

So far, the zonal and meridional components of the wind have been compared separately. It is also of interest to compare the radar and lidar winds in terms of speed (magnitude) and direction. Figure 4 shows the distribution of the radar/lidar wind speed ratio. The median of this distribution is 0.95. A median of 1.0, would indicate that radar wind speed exceeded the lidar wind speed in 50% of the measurements (and vice versa). To

Figure 4

test whether or not the observed value is significantly different from 1.0, we applied the Wilcoxin signed-rank sum test to the quantity $1.0 - (\text{speed ratio})$, which would have a median of 0 if the median speed ratio is 1.0. The test indicates that the observed value of 0.95 is not significantly different from 1.0 at the 5% level.

Figure 5 shows the distribution of radar/lidar wind direction differences, in degrees. The mean wind direction difference is 3.4° , and a 99% bootstrap confidence interval is $[-6.3^\circ, 13.8^\circ]$. The median of the direction difference distribution is -2.8° . A Wilcoxin test indicates that the median difference is not significant at the 5% level. The actual probability of observing a median difference this large or larger, if the underlying population median is 0° , is 15%. Hence, we conclude that the wind direction differences are not significantly different from 0° .

Figure 5

The summary statistics described above include data from all altitudes. The altitude dependence of the statistics is summarized next. Figure 6 shows how the variances and covariances depend on altitude in the 5 layers spanning 80-100 km. The number of radar/lidar sample pairs represented in these statistics is between 82 and 96 in the middle three layers, but only 12 and 55 at the lowest and highest layers, respectively. Thus, the results for the lowest layer have relatively large uncertainty. Note, again, that the lidar variance exceeds the radar variance at most altitudes and that the radar/lidar covariance is nearly equal to the radar variance at all altitudes. Figure 7 shows the radar/lidar correlation coefficients derived from the data plotted in Figure 6, and illustrates that correlation is high at all altitudes, and is in the range 0.79-0.94.

Figure 6

Figure 7

Finally, Figure 8 shows the median absolute value of the radar/lidar wind differences (plotted with filled triangles) and rms difference (plotted with filled squares). The median

Figure 8

absolute differences are 7-8 m/s (meridional) and 8-11 m/s (zonal) at the three central height bins spanning 84-96 km. Somewhat larger values appear for the meridional component at the highest altitude bin (96-100 km), and for the zonal component at the lowest altitude bin (80-84 km). Within the 80-96 km height range the rms differences are \sim 12-14 m/s, and \sim 13-17 m/s. Higher rms differences are observed at the highest altitude bin (96-100 km).

4. Interpretation

The lidar photocounts are highest just above 90 km and the meteor echo occurrence peaks at 90 km. Thus, winds estimated by the two instruments will have the smallest instrumental errors near 90 km and the errors will tend to be larger at significantly lower or higher altitudes. In addition, it is known that spatial and temporal fluctuations of the wind field associated with gravity waves tend to increase with altitude, especially above 96 km (e.g. *Gardner et al.*, 2002). It is likely that these effects account for the fact that the radar/lidar median and rms differences tend to be smallest, and the correlation coefficients largest, within the central height bin (spanning 88-92 km) and the fact that the rms difference increases more quickly above that range than below it. Additional physical mechanisms related to electrodynamicity may operate to structure and move meteor trails at altitudes near and above 95 km, and could also contribute to the larger rms differences observed at the highest bin (e.g. *Oppenheim et al.*, 2003).

In the combined (as summarized in Table 2) and height-sorted data sets (as summarized in Figure 6), the radar/lidar wind component covariances are very nearly equal to the radar variances. In addition, in the combined data set, the lidar variance exceeds the radar variance by 12% (meridional) and 7% (zonal). When sorted by height, the lidar

variance exceeds the radar variance in 4 out of 5 height bins for both meridional and zonal components, by as much as 20%. These characteristics are consistent with the results and interpretation published by *Liu et al.* (2002) for the earlier comparison at SOR. In that study, zonal and meridional components were compared separately at 2 heights, and the lidar variance exceeded the radar variance by 14-29% in 3 out of the 4 cases. As noted earlier, and discussed in *Liu et al.*, the larger variance of lidar winds is consistent with the fact that the lidar technique is sensitive to wind perturbations within a larger range of horizontal wavenumbers. This situation can be modeled by decomposing the fluctuating (zero-mean) component of the wind field into two statistically independent components, one having relatively large horizontal scale size (v_{ls}) that is resolved by both the radar and lidar and the other having a small horizontal scale size that is resolved only by the lidar (v_{ss}), i.e. the estimated radar and lidar wind components may be written as follows:

$$v_R = v_{ls} + \delta v_R, \quad (4)$$

and

$$v_L = v_{ls} + v_{ss} + \delta v_L, \quad (5)$$

where δv_R and δv_L represent radar and lidar estimation errors, respectively. Assuming that all terms have zero mean, then variances are equal to mean-square values, and the radar variance is

$$\langle v_R^2 \rangle = \langle v_{ls}^2 \rangle + \langle \delta v_R^2 \rangle. \quad (6)$$

The lidar variance is

$$\langle v_L^2 \rangle = \langle v_{ls}^2 \rangle + \langle v_{ss}^2 \rangle + \langle \delta v_L^2 \rangle, \quad (7)$$

and the radar/lidar covariance is

$$\langle v_R v_L \rangle = \langle v_{ls}^2 \rangle. \quad (8)$$

The measured radar variance is nearly equal to radar/lidar covariance at all altitudes, which implies that $\langle v_{ls}^2 \rangle \gg \langle \delta v_R^2 \rangle$, i.e. radar variance is dominated by large-scale geophysical wind fluctuations which are also sensed by the lidar. The small difference between the radar variance and the radar/lidar covariance reflects the mean square radar estimation error ($\langle \delta v_R^2 \rangle$). For the combined data set, the radar variance exceeds the radar/lidar covariance by $50 \text{ m}^2/\text{s}^2$ (meridional) and $94 \text{ m}^2/\text{s}^2$ (zonal). The inferred estimation errors are $\sqrt{50} \simeq 7.1 \text{ m/s}$ (meridional) and $\sqrt{94} \simeq 9.7 \text{ m/s}$ (zonal). These values are remarkably consistent with the median standard errors derived independently from the weighted least squares fitting procedure, which are 7.6 m/s (meridional) and 9.3 m/s (zonal).

When all altitudes are considered together, the lidar variance exceeds the radar/lidar covariance by $202 \text{ m}^2/\text{s}^2$ (meridional) and $185 \text{ m}^2/\text{s}^2$ (zonal). Since the median lidar estimation errors are only $\sim 3\text{-}4 \text{ m/s}$, the excess lidar variance is almost entirely due to geophysical wind fluctuations with horizontal scales that are smaller than $\sim 200 \text{ km}$, and therefore too small to be resolved by the radar. Our results suggest that the variance of this small-scale component of the horizontal wavenumber spectrum is $\langle v_{ss}^2 \rangle \simeq 200 \text{ m}^2/\text{s}^2$.

We conclude our interpretation of the results with a summary of the error budget for the radar/lidar differences. According to our model for the second moments of the radar and lidar winds, the rms difference is

$$\sqrt{\langle (v_L - v_R)^2 \rangle} = \sqrt{\langle v_{ss}^2 \rangle + \langle \delta v_R^2 \rangle + \langle \delta v_L^2 \rangle}. \quad (9)$$

We have shown that the dominant term in this error budget is $\langle v_{ss}^2 \rangle$, which was estimated to be $\sim 200 \text{ m}^2/\text{s}^2$. Thus, even in the absence of the estimation errors associated with the radar and lidar instruments, an rms difference $\sim \sqrt{200} = 14 \text{ m/s}$ is expected, due to the inherent mismatch between the horizontal wavenumber response functions. Taking the medians of the standard errors provided by the radar and lidar wind estimation algorithms as representative values for the mean square radar and lidar estimation errors, the estimation errors are $8^2 \text{ m}^2/\text{s}^2$ and $3.5^2 \text{ m}^2/\text{s}^2$ for the radar and lidar, respectively. When these contributions are added, the expected rms difference increases to $\sim 16.6 \text{ m/s}$, commensurate with our observations.

5. Summary and Conclusion

In summary, the joint radar and lidar data set has been examined carefully for evidence of significant differences in mean meridional and zonal wind components and wind direction. No statistically significant differences were discovered. The distribution of the radar/lidar wind speed ratio was examined for evidence of any tendency for one instrument to systematically measure larger or smaller wind speeds relative to the other, and no evidence for such a tendency was found. The comparison presented herein suggests that the rms differences observed between radar and lidar wind measurements are mainly due the fact that the instruments view the wind field through different horizontal wavenumber filters, and that the magnitude of the differences reflects the spectral density of the horizontal wavenumber spectrum at scales smaller than $\sim 200 \text{ km}$ and within the range of temporal frequencies and vertical wavenumbers resolved by the 1 hour and 4 km time and altitude resolution of the data.

The rms radar/lidar wind differences are smaller than those reported for the earlier comparison between the UIUC Na lidar and a meteor radar. In particular, *Liu et al.* (2002) reported an average rms difference of 20 m/s at 86 km and 93 km, and correlation coefficients in the range 0.63-0.70 at these two altitudes for comparisons at SOR in New Mexico. In contrast, the rms difference reported here is in the range 12-17 m/s in the 80-96 km range, and correlations are in the range 0.79-0.94 at these altitudes. The meteor radar at Maui operates in a more favorable radio-frequency environment than the radar at SOR, with less interference and correspondingly higher meteor echo occurrence rates. Also, the lidar was pointed only 10° degrees off of zenith for the SOR campaign, whereas the off-zenith angle was 30° at Maui. For equal photon counts the instrumental errors will therefore be larger by $\sin(30^\circ)/\sin(10^\circ)=2.9$ at SOR. Generally, photon counts per pulse were larger at SOR by a factor of $\sim 3 - 5$, but the pulse repetition rate was 60% smaller. Overall, the instrumental errors were ~ 2 times larger at SOR. Thus, both instruments achieved smaller estimation errors at Maui. Another factor which undoubtedly acts to increase the correlation coefficients at Maui is the large amplitude of the diurnal and semi-diurnal oscillations at this location relative to SOR. This provides a large common-mode signal for the radar and lidar which will tend to decrease the de-correlating influence of estimation errors and wind perturbations with relatively small horizontal scales that can be resolved by the lidar but not the radar.

Acknowledgments. The material reported in this paper is based on work supported by the U.S. National Science Foundation under grants ATM 00-03182, ATM 00-3198. We appreciate valuable comments and support from Chet Gardner and Gary Swenson. Support by the Air Force Research Laboratory for the telescope utilization, and by Boe-

ing staff for telescope operations is appreciated as a major contribution to this study. SJF especially thanks Russ Taft and Jake Barros for their support of the meteor radar operations.

References

- B. Efron and R. J. Tibshirani, An Introduction to the Bootstrap, *CRC Press*, 1993.
- C. S. Gardner, Yucheng Zhao, Alan Z. Liu, Atmospheric stability and gravity wave dissipation in the mesopause region, *J. Atmos. Sol. Terr. Phys.*, *64*, 923-929, 2002.
- W. K. Hocking, B. Fuller, B. Vandeppeer, Real-time determination of meteor-related parameters utilizing modern digital technology, *J. Atmos. Sol. Terr. Phys.*, *63*, 155-169, 2001.
- J. Jones, A. R. Webster, W. K. Hocking, An improved interferometer design for use with meteor radars, *Radio Science*, *33*, 55-65, 1998.
- A. Z. Liu, W. K. Hocking, S. J. Franke, T. Thayaparan, Comparison of Na lidar and meteor radar wind measurements at Starfire Optical Range, NM, USA, *J. Atmos. Sol. Terr. Phys.*, *64*, 31-20, 2002.
- M. M. Oppenheim, L. P. Dyrud, and A. F. vom Endt, Plasma instabilities in meteor trails: 2-D simulation studies, *J. Geophys. Res.*, *108*, 1064, 2003.
- F. Wilcoxon, Individual Comparisons by Ranking Methods, in Breakthroughs in Statistics, Volume II, ed. S. Kotz and N. L. Johnson, Springer-Verlag, 1992.

Table 1. Parameters used in the error model (equation (3)).

σ_θ	2°
σ_r	1.33 km
σ_u	10 m/s
σ_w	1 m/s
σ_S	7 m/s/km

Table 2. Statistical moments of horizontal wind components for all coincident data points in the 82-98 km altitude range. The angle brackets $\langle \rangle$ represent an average over all coincident radar/lidar samples. Symbols u_L , and u_R represent the zonal component of lidar and radar winds, respectively, whereas v_L , and v_R represent the meridional components. The symbol γ is used to represent the correlation coefficients, i.e. $\gamma(x, y) = Cov(x, y) / \sqrt{Var[x]Var[y]}$.

Meridional	Value	Zonal	Value
# of coincident samples	341	# of coincident samples	326
$\langle v_R^i \rangle$	13.1 m/s	$\langle u_R^i \rangle$	-3.8 m/s
$\langle v_L^i \rangle$	12.7 m/s	$\langle u_L^i \rangle$	-4.4 m/s
median[$v_L^i - v_R^i$]	0.8 m/s	median[$u_L^i - u_R^i$]	-0.2 m/s
Var[v_R^i]	1268 m ² /s ²	Var[u_R^i]	1217 m ² /s ²
Var[v_L^i]	1420 m ² /s ²	Var[u_L^i]	1308 m ² /s ²
Cov[v_R^i, v_L^i]	1218 m ² /s ²	Cov[u_R^i, u_L^i]	1123 m ² /s ²
$\gamma(v_R^i, v_L^i)$	0.91	$\gamma(u_R^i, u_L^i)$	0.89
$\sqrt{\langle (v_R^i - v_L^i)^2 \rangle}$	15.9 m/s	$\sqrt{\langle (u_R^i - u_L^i)^2 \rangle}$	16.7 m/s
median[$ v_R^i - v_L^i $]	8.4 m/s	median[$ u_R^i - u_L^i $]	9.0 m/s

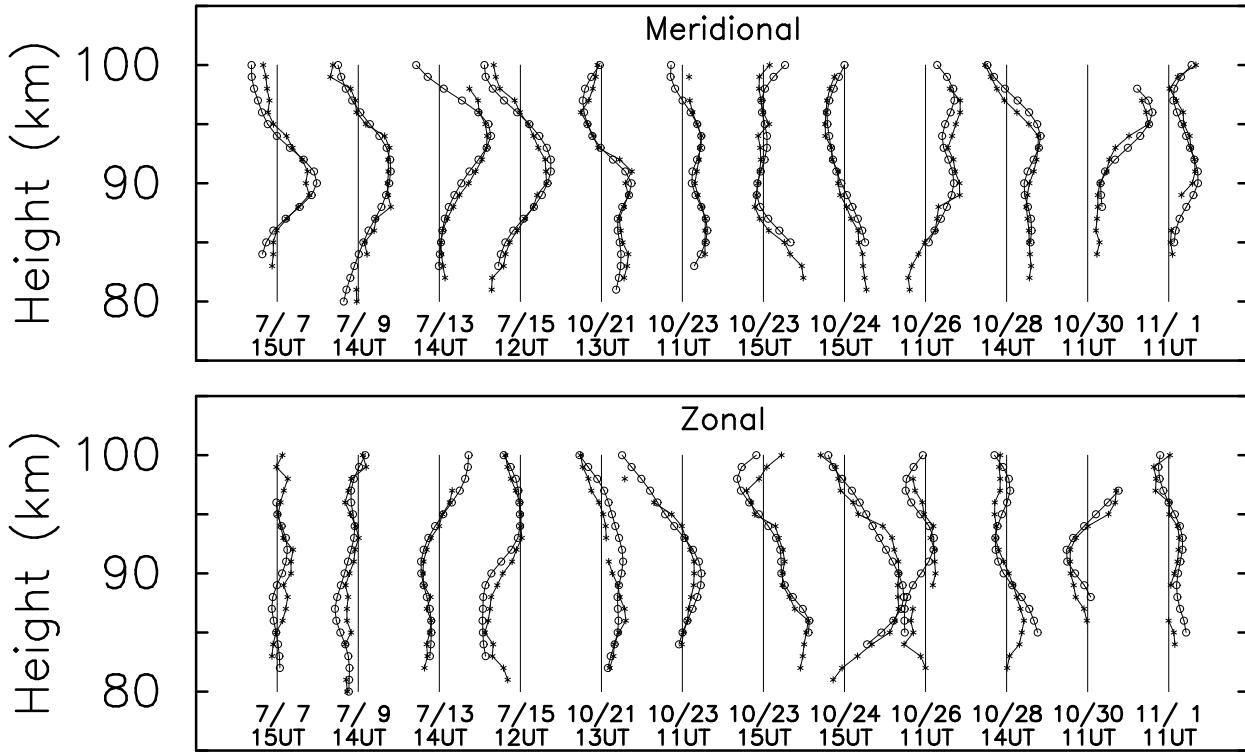


Figure 1. Sample meridional (top) and zonal (bottom) wind profiles collected during the July 2002 and October 2003 campaigns. Lidar profiles are marked with circles (\circ) and radar profiles are marked with asterisks (*). The profiles are scaled such that the horizontal distance between vertical lines corresponds to 150 m/s.

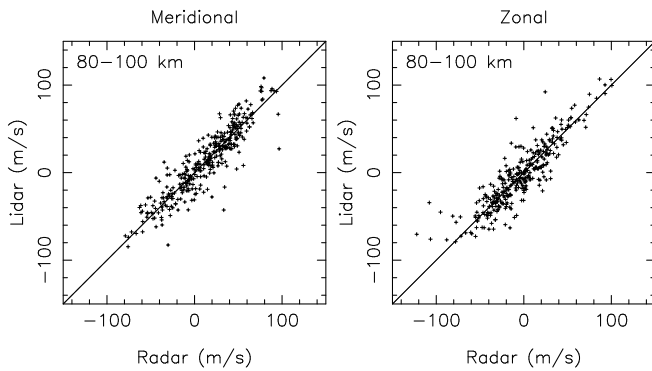


Figure 2. Scatter plots for all coincident radar and lidar measurements in 80-100 km altitude range.

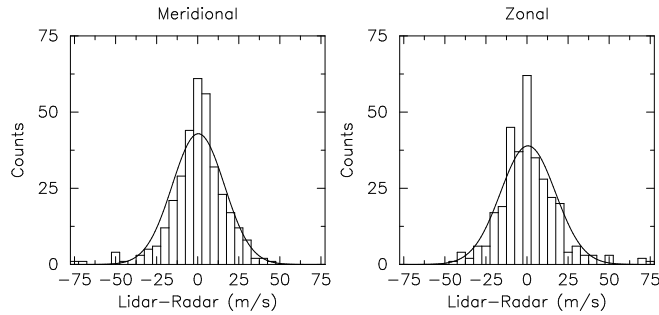


Figure 3. Histograms of radar/lidar wind component differences within the 80-100 km altitude range. See Table 2 for summary statistics of the wind component differences. The smooth curves represent normal distributions with mean and variance equal to the sample mean and variance.

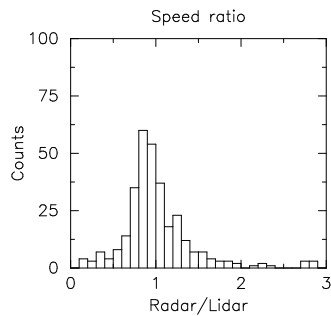


Figure 4. Histograms of radar/lidar wind speed ratio within the 80-100 km altitude range. The median speed ratio is 0.95.

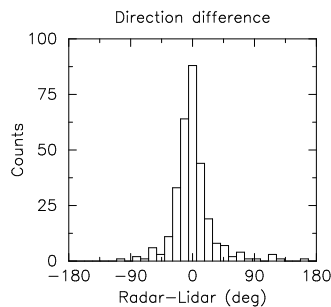


Figure 5. Histograms of radar-lidar wind vector direction differences, in degrees, within the 80-100 km altitude range. The mean direction difference is -3.4° and a 99% confidence interval derived using a bootstrap calculation is $[-6.3^\circ, 13.8^\circ]$.

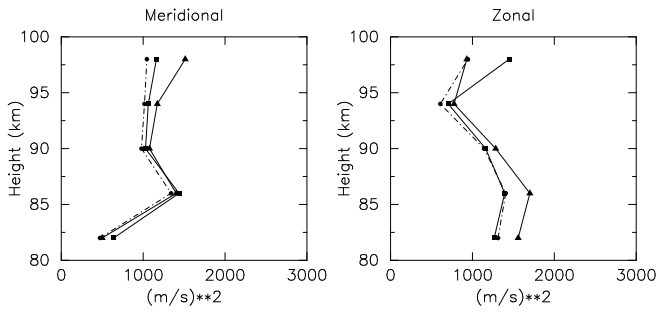


Figure 6. Variance of radar (solid line with squares) and lidar (solid line with triangles) winds and the covariance (dash-dot line with circles) as a function of height.

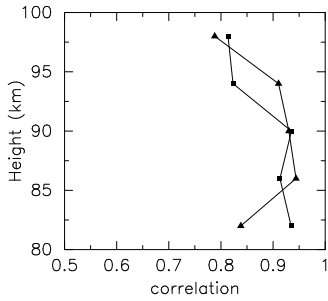


Figure 7. Correlation coefficient for meridional (triangles) and zonal (squares) radar/lidar wind components as a function of height.

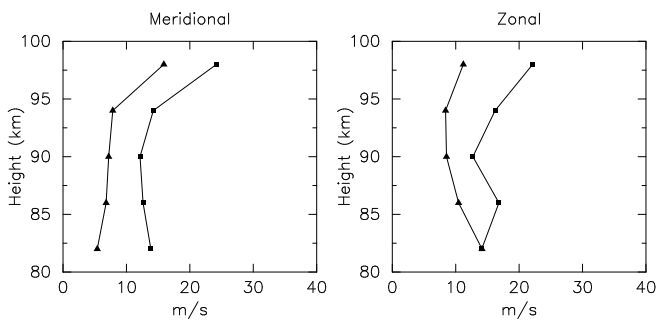


Figure 8. Median absolute difference (triangles) and rms difference (squares) between lidar and radar wind components vs height.